

## NRC Publications Archive Archives des publications du CNRC

### The role of Al<sup>3+</sup>-based aqueous electrolytes in the charge storage mechanism of MnO<sub>x</sub> cathodes

Balland, Véronique; Mateos, Mickaël; Singh, Arvinder; Harris, Kenneth D.; Laberty-Robert, Christel; Limoges, Benoît

This publication could be one of several versions: author's original, accepted manuscript or the publisher's version. / La version de cette publication peut être l'une des suivantes : la version prépublication de l'auteur, la version acceptée du manuscrit ou la version de l'éditeur.

For the publisher's version, please access the DOI link below. / Pour consulter la version de l'éditeur, utilisez le lien DOI ci-dessous.

#### **Publisher's version / Version de l'éditeur:**

<https://doi.org/10.1002/sml.202101515>

*Small*, 2021-05-06

#### **NRC Publications Archive Record / Notice des Archives des publications du CNRC :**

<https://nrc-publications.canada.ca/eng/view/object/?id=5a5ef50b-0efc-4c84-9fe7-90a5256afdf3>

<https://publications-cnrc.canada.ca/fra/voir/objet/?id=5a5ef50b-0efc-4c84-9fe7-90a5256afdf3>

Access and use of this website and the material on it are subject to the Terms and Conditions set forth at

<https://nrc-publications.canada.ca/eng/copyright>

READ THESE TERMS AND CONDITIONS CAREFULLY BEFORE USING THIS WEBSITE.

L'accès à ce site Web et l'utilisation de son contenu sont assujettis aux conditions présentées dans le site

<https://publications-cnrc.canada.ca/fra/droits>

LISEZ CES CONDITIONS ATTENTIVEMENT AVANT D'UTILISER CE SITE WEB.

**Questions?** Contact the NRC Publications Archive team at

PublicationsArchive-ArchivesPublications@nrc-cnrc.gc.ca. If you wish to email the authors directly, please see the first page of the publication for their contact information.

**Vous avez des questions?** Nous pouvons vous aider. Pour communiquer directement avec un auteur, consultez la première page de la revue dans laquelle son article a été publié afin de trouver ses coordonnées. Si vous n'arrivez pas à les repérer, communiquez avec nous à PublicationsArchive-ArchivesPublications@nrc-cnrc.gc.ca.

# Revisiting the role of Al<sup>3+</sup>-based aqueous electrolytes in the charge storage mechanism of MnO<sub>x</sub> cathodes

*Véronique Balland,<sup>†,\*</sup> Mickaël Mateos,<sup>†</sup> Kenneth D. Harris,<sup>‡,§</sup> Benoît Limoges<sup>†,\*</sup>*

<sup>†</sup> Université de Paris, Laboratoire d'Electrochimie Moléculaire, UMR CNRS 7591, F-75013  
Paris, France.

<sup>‡</sup> National Research Council Canada, Nanotechnology Research Centre, Edmonton, Alberta, T6G  
2M9, Canada

<sup>§</sup> Department of Mechanical Engineering, University of Alberta, Edmonton, Alberta, T6G 2V4,  
Canada

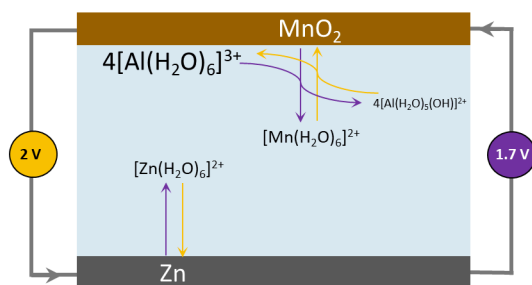
AUTHOR INFORMATION

**Corresponding Author**

\* [veronique.balland@u-paris.fr](mailto:veronique.balland@u-paris.fr), \* [limoges@u-paris.fr](mailto:limoges@u-paris.fr)

ABSTRACT. Rechargeable aqueous aluminum batteries are the subject of growing interest, but the charge storage mechanisms at manganese oxide-based cathodes remain poorly understood with as many mechanisms as studies. Here, we use an original *in situ* spectroelectrochemical methodology to unambiguously demonstrate that the reversible proton-coupled  $\text{MnO}_2$ -to- $\text{Mn}^{2+}$  conversion is the main charge storage mechanism occurring at  $\text{MnO}_2$  cathodes over a range of slightly acidic  $\text{Al}^{3+}$ -based aqueous electrolytes. In  $\text{Zn}/\text{MnO}_2$  assemblies, this mechanism is associated with high gravimetric capacity and discharge potentials, up to  $560 \text{ mAh}\cdot\text{g}^{-1}$  and  $1.76 \text{ V}$  respectively, attractive efficiencies ( $CE > 98.5 \%$  and  $EE > 80\%$ ) and excellent cyclability ( $> 750$  cycles at  $10 \text{ A}\cdot\text{g}^{-1}$ ). Finally, we conducted a critical analysis of the data previously published on  $\text{MnO}_x$  cathodes in  $\text{Al}^{3+}$ -based aqueous electrolytes and identified the universal charge storage mechanism: reversible electrodisolution/electrodeposition of  $\text{MnO}_2$ .

## TOC GRAPHICS



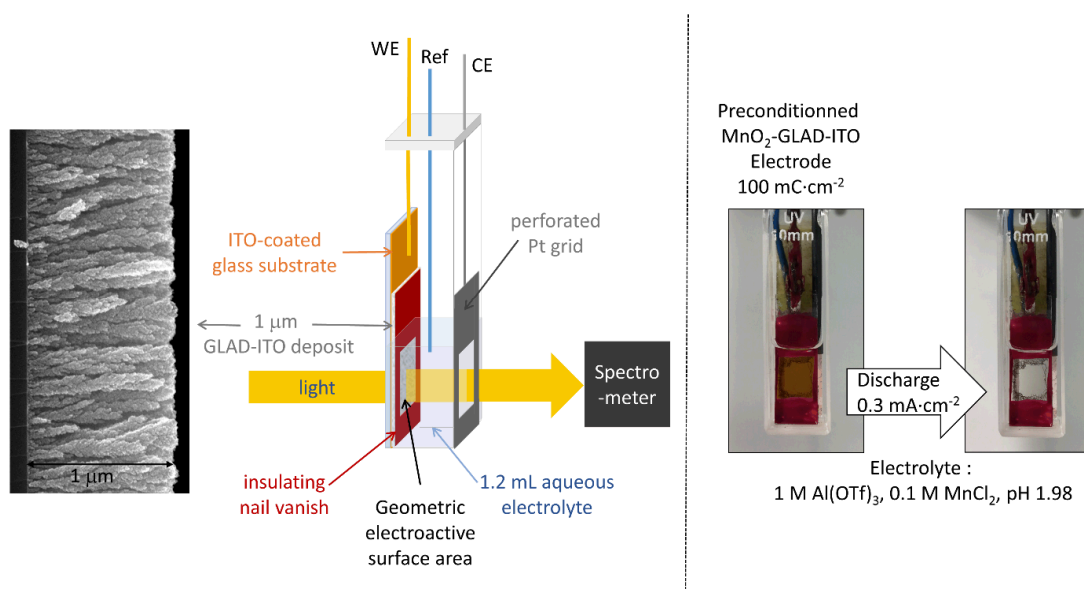
Insertion of earth-abundant multivalent (MV) metal cations (*e.g.*,  $\text{Mg}^{2+}$ ,  $\text{Zn}^{2+}$  and  $\text{Al}^{3+}$ ) into host electrode materials is currently the subject of much attention due to the promising potential to go “beyond lithium”. This is especially true with regard to the development of new insertion-based rechargeable aqueous batteries, which are currently under intensive study due to cost, safety and eco-sustainability considerations.<sup>1,2</sup> However, the real ability of multivalent cations to reversibly insert into redox-active materials, especially metal oxide-based hosts, is still uncertain.<sup>3</sup> Indeed, it has long been believed that the strong electrostatic interaction of MV cations with metal oxide lattices considerably hinders solid-state diffusivity,<sup>4</sup> leading to low electrochemical activity even in the presence of a strong thermodynamic driving force. Moreover, the high solvation energy of MV cations, especially in water, is an additional insertion barrier, adding to the difficulties of MV-ion insertion. Despite all of this, numerous recent works report the reversible insertion of MV cations into metal oxides in the presence of water, and under these conditions, they demonstrate electrochemical performances much better than in pure organic electrolytes.<sup>5-7</sup> However, a growing number of recent studies propose that the attractive performances observed with aqueous MV-ion batteries result from the reversible insertion of protons into the host electrode rather than MV cations. This has been evidenced in particular for  $\text{VO}_2$ ,<sup>8</sup>  $\text{V}_2\text{O}_5$ ,<sup>9</sup>  $\text{Na}_3\text{V}_2(\text{PO}_4)_2\text{F}_3$ ,<sup>10</sup> and  $\text{TiO}_2$ <sup>11</sup> electrode materials cycled in either mild acidic  $\text{Zn}^{2+}$ - or  $\text{Al}^{3+}$ -based aqueous electrolytes. Moreover, in our previous work on  $\text{TiO}_2$ , we demonstrated that the source of protons in mild aqueous electrolytes was neither water nor  $\text{H}_3\text{O}^+$ , but the hexaaquo MV complexes (*e.g.*,  $[\text{Zn}(\text{H}_2\text{O})_6]^{2+}$ ,  $[\text{Al}(\text{H}_2\text{O})_6]^{3+}$ ) which spontaneously form in water to produce weak Brønsted acids.<sup>11</sup> More recently, we have also shown that the hexaaquo cations  $[\text{Zn}(\text{H}_2\text{O})_6]^{2+}$  and  $[\text{Mn}(\text{H}_2\text{O})_6]^{2+}$ , commonly present in the aqueous electrolytes of Zn/MnO<sub>2</sub> batteries, can act as proton sources to trigger the electrodisolution of MnO<sub>2</sub> into  $\text{Mn}^{2+}$ .<sup>12</sup> These studies underline the crucial, but little-

known role played by the weak acidity of hydrated MV ions on the charge storage mechanisms at metal oxide electrodes. An illustration is provided by the trivalent  $\text{Al}^{3+}$  cation, which has recently been promoted for “rechargeable aqueous aluminium batteries”, wherein an aluminium (or zinc) anode is paired with a  $\text{MnO}_x$  cathode in an  $\text{Al}^{3+}$ -based aqueous electrolyte.<sup>13–18</sup> A collective issue with these works, however, is the disparate variety of charge storage mechanisms and cathode compositions that are proposed. Indeed, some works suggest the reversible insertion of MV cations ( $\text{Al}^{3+}$  or  $\text{Zn}^{2+}$ ) into either the pristine  $\text{K}_x\text{MnO}_2$  phase<sup>16</sup> or an  $\text{Al}_x\text{MnO}_2$  phase generated from a solid  $\text{Mn}_3\text{O}_4$ ,<sup>14</sup>  $\text{MnO}$ <sup>18</sup> or  $\text{MnO}_2$ <sup>17</sup> precursor. Other reports assume a reversible conversion process, either solid-solid (*i.e.*,  $\text{MnO}_2$ -to- $\text{Mn}_3\text{O}_4$ )<sup>13</sup> or solid-liquid (*i.e.*,  $\text{Al}_x\text{MnO}_2$ -to- $\text{Mn}^{2+}$ ),<sup>15</sup> without clearly describing the role and source of protons.

In light of the numerous and contradictory mechanistic propositions, our objective with the present work is to decipher the exact role of  $\text{Al}^{3+}$  ions in the reversible charge storage mechanism of  $\text{MnO}_x$  cathodes immersed in  $\text{Al}^{3+}$ -based aqueous electrolytes. As we will see, our results unambiguously support a mechanism based on the reversible proton-coupled electrodisolution of solid  $\text{MnO}_x$  materials into soluble  $\text{Mn}^{2+}$  ions for a wide range of  $\text{Al}^{3+}$ -based electrolyte compositions, and they challenge the previously-reported charge storage mechanisms which are critically reviewed here.<sup>13–18</sup>

In the present work,  $\text{MnO}_x$  is quantitatively monitored during galvanostatic cycling by *in operando* UV-visible spectroelectrochemistry. This method was previously used to characterize amorphous  $\text{MnO}_2$  within a 3D mesoporous transparent electrode (*i.e.*, a 1  $\mu\text{m}$ -thick nanostructured ITO film deposited by glancing angle deposition (GLAD), over a flat ITO-coated glass substrate – see Scheme 1).<sup>12,19</sup> Here, we prepare similar  $\text{MnO}_2$ -GLAD-ITO electrodes (see Experimental Section for details and Fig. S1 and S2)<sup>19</sup> by systematically applying 100  $\text{mC}\cdot\text{cm}^{-2}$  to the

nanocolumnar GLAD-ITO electrodes, which is equivalent to  $48 \pm 1 \mu\text{g}\cdot\text{cm}^{-2} \text{MnO}_2$ .<sup>19</sup> XRD and XPS analysis of the electrodeposited material show that  $\text{MnO}_2$  is amorphous and characterized by an average Mn oxidation state of 3.86.<sup>19</sup> Accordingly, the maximal theoretical gravimetric capacity of these  $\text{MnO}_2$ -GLAD-ITO electrodes is  $574 \text{ mA}\cdot\text{h}\cdot\text{g}^{-1}$ . Their electrochemical reactivity was examined with/without  $\text{Al}^{3+}$  in a three-electrode cell configuration in different aqueous electrolytes adjusted to pH 2.0 (see Table S1 for chemical compositions). The spectroelectrochemical data associated with the first galvanostatic discharges are given in Fig. 1A and 1B.



**Scheme 1.** Left: schematic of the *in operando* spectroelectrochemical setup used to monitor a  $\text{MnO}_2$ -loaded GLAD-ITO electrode (made of a 1- $\mu\text{m}$  thick transparent nanostructured film of GLAD-ITO). Right: photographs of the spectroelectrochemical cell taken at the beginning and end of a galvanostatic discharge experiment performed at a GLAD-ITO electrode loaded *ex situ*.

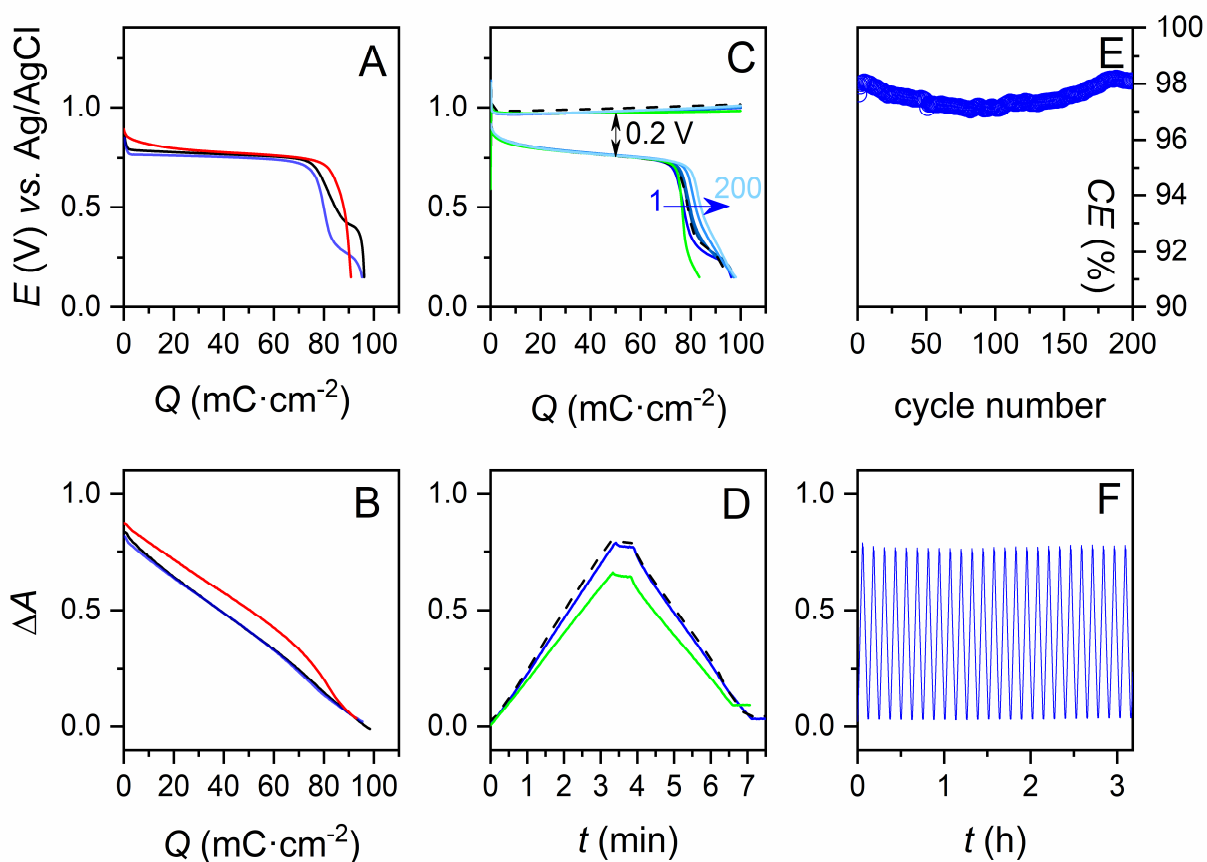
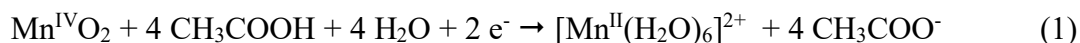


**Figure 1.** *In operando* spectroelectrochemical characterization of  $\text{MnO}_2$ -GLAD-ITO electrodes in different aqueous electrolytes (adjusted to pH 2). (A) Galvanostatic curves (rate:  $0.3 \text{ mA}\cdot\text{cm}^{-2}$ ) and (B) absorbance variations concomitantly recorded during the first discharge of a  $\text{MnO}_2$ -GLAD-ITO electrode (loaded *ex situ* with a deposited charge of  $100 \text{ mC}\cdot\text{cm}^{-2}$ ) immersed in the following electrolytes: (red) 1 M acetic acid + 0.1 M  $\text{MnCl}_2$  + 2 M  $\text{KCl}$ , (blue) 1 M  $\text{Al}(\text{OTf})_3$  + 0.1 M  $\text{MnCl}_2$ , and (black) 1 M  $\text{AlCl}_3$  + 0.1 M  $\text{MnCl}_2$ . (C) Galvanostatic charge/discharge curves (rate:  $0.3 \text{ mA}\cdot\text{cm}^{-2}$ ) and (D, F) absorbance variations concomitantly recorded at a GLAD-ITO electrode cycled in an aqueous electrolyte containing: (blue) 1 M  $\text{Al}(\text{OTf})_3$  + 0.1 M  $\text{MnCl}_2$ , (dashed black) 1 M  $\text{Al}(\text{OTf})_3$  + 0.1 M  $\text{MnCl}_2$ , and (green) 1.4 M  $\text{Al}(\text{OTf})_3$  + 7.1 mg/L  $\text{MnO}$  (see text for details). (E) Coulombic efficiencies (CE) recovered from the continuous galvanostatic experiment reported in (C) and (F).

In a 1 M acetic acid (pH 2.0) electrolyte, the galvanostatic discharge curve is characterized by a well-defined single plateau (red line in Fig. 1A), leading to an areal discharge capacity ( $C_d$ ) of 92  $\text{mC}\cdot\text{cm}^{-2}$  (Table S1) close to the *ex situ* deposited charge of 100  $\text{mC}\cdot\text{cm}^{-2}$  (thus a Coulombic efficiency of  $CE = 92\%$ ). Concomitantly, the absorbance of the electrode decreases almost linearly to near zero (red line in Fig. 1B). These observations are in line with those we have recently reported<sup>19</sup> in a 1 M acetate buffer of pH 5 and support the following proton-coupled electron transfer reaction, in which acetic acid is involved as a proton donor:



The near complete electrodisolution of  $\text{MnO}_2$  is further confirmed by the low  $m_{\text{MnO}_2}$  value obtained for the discharged electrode (Table S1), indicating that only  $\sim 4\%$  of the initially electrodeposited Mn remains on the electrode. As a result, the discharge gravimetric capacity is 530  $\text{mA}\cdot\text{h}\cdot\text{g}^{-1}$ , close to the theoretical value.

The half-discharge potential ( $E_d$ ) of 0.74 V (vs. Ag/AgCl) is significantly higher than that previously reported in a 1 M acetate buffer of pH 5 ( $E_d = 0.50$  V).<sup>12,19</sup> This can be easily explained from the lower electrolyte pH here and the Nernst equation derived from reaction 1 (see eq. S1).<sup>12</sup> However, to accurately interpret the  $E_d$  value, it is important to consider that the local pH at the  $\text{MnO}_2$ /electrolyte interface can differ from the bulk and is indeed expected to rise significantly during the  $\text{MnO}_2$  electrodisolution (according to the stoichiometry of reaction 1). Using eq. S1 and assuming that the process remains near thermodynamic equilibrium, the  $E_d$  value of 0.74 V translates into a local pH of  $\sim 3$ , thus slightly higher than the bulk pH 2. This agrees with a local conversion of acetic acid into acetate, which, as a function of their respective local activities and  $\text{p}K_a$  (4.74), determine the local pH (see SI for details).

It is worth noting that at pH 2, the concentration of free protons (*i.e.*,  $\text{H}_3\text{O}^+$ ) remains too low ( $\sim 10^{-2}$  M) to trigger the reductive electrodisolution of  $\text{MnO}_2$  in an inert KCl electrolyte (see Fig. S4 and associated text), whereas at pH 1, the  $\text{H}_3\text{O}^+$  concentration becomes sufficient ( $\sim 0.1$  M) to complete the proton-coupled electrodisolution of  $\text{MnO}_2$  (see Fig. S4 and Table S1). This behaviour is consistent with recent reports for rechargeable aqueous Zn/ $\text{MnO}_2$  batteries operating in strongly acidic electrolytes.<sup>20,21</sup> As a consequence for further study, we deliberately avoided the overly concentrated  $\text{Al}^{3+}$ -based electrolytes (common in the literature) as they leads to very low pHs (Table S2) and participation of  $\text{H}_3\text{O}^+$  in the discharge process. In Fig. 1A and 1B, the data recorded during the first galvanostatic discharge of  $\text{MnO}_2$ -GLAD-ITO electrodes in 1 M  $\text{Al}(\text{OTf})_3$  and 1 M  $\text{AlCl}_3$  aqueous electrolytes (pH 2) are also overlaid. The shapes and positions of the discharge and absorption curves are almost identical to those recorded in the 1 M acetic acid, the only difference being the appearance of a poorly-defined secondary discharge plateau, located at a lower potential. We do not believe these secondary plateaus are linked to aluminium ions in the electrolyte since they were previously observed in an  $\text{Al}^{3+}$ -free acidic electrolyte.<sup>21</sup> Alternatively, we suspect it could be related to the denucleation process, which may be more difficult at the end of the discharge. For either  $\text{Al}^{3+}$ -based electrolyte, a full recovery of the electrode transparency was observed (see pictures in Scheme 1), demonstrating full electrodisolution of  $\text{MnO}_2$ . This was also corroborated by both the high CE > 96% and small  $m_{\text{MnO}_2}$  values after discharge (see Table S1). Accordingly, an exploitable gravimetric capacity as high as  $550 \text{ mA}\cdot\text{h}\cdot\text{g}^{-1}$  could be achieved, almost identical to the value in 1 M acetic acid. These observations lead to the irrefutable conclusion that we are dealing with a two-electron  $\text{MnO}_2$ -to- $\text{Mn}^{2+}$  conversion mechanism, involving protons (or proton donors) as the charge carriers.

Another interesting feature of the discharge curves in Fig. 1A is their almost identical half-discharge potential values (Table S1), which indicates similar local pHs at the MnO<sub>2</sub> surfaces regardless the nature of the electrolyte. This implies that the proton donors involved in the conversion reactions are weak Brønsted acids of similar strength (*i.e.*, close p*K*<sub>a</sub>). Given that the hexaaquo complex [Al(H<sub>2</sub>O)<sub>6</sub>]<sup>3+</sup> has a weak Brønsted acidity (p*K*<sub>a</sub> = 4.9)<sup>22</sup> comparable to that of acetic acid (p*K*<sub>a</sub> = 4.76), we propose by analogy to reaction 1, the following proton-coupled MnO<sub>2</sub>-reductive electrodisolution reaction 2 in the Al<sup>3+</sup>-based aqueous electrolytes:



Once completely discharged, the electrodes were subjected to a galvanostatic charge of 100 mC·cm<sup>-2</sup> at a rate of 0.5 mA·cm<sup>-2</sup>. The data recorded in 1 M Al(OTf)<sub>3</sub> containing 0.1 M MnCl<sub>2</sub> are reported in Fig. 1C to 1F (blue curves). During the charge, the potential rapidly stabilizes at 0.98 V, while the absorbance of the electrode increases linearly (Fig. 1D), confirming a steady electrodeposition of MnO<sub>2</sub> to an amount close to that achieved for the electrodes loaded *ex situ*. Interestingly, similar results were obtained with a fresh GLAD-ITO electrode charged *in situ* in the same electrolyte (see black dashed lines in Fig. 1C and 1D), confirming that the MnO<sub>2</sub> electrodeposition remains effective in the Al<sup>3+</sup>-based electrolyte.

Owing to the conversion mechanism, the electrodeposition of MnO<sub>2</sub> requires the presence of soluble Mn<sup>2+</sup> ions in the electrolyte. This is commonly achieved by adding a highly soluble inorganic Mn<sup>2+</sup> salt to the electrolyte. However, as shown below, it can also be achieved from a solid precursor such as MnO, calling into question the recent work of Yan *et al.* on the reversible insertion of Al<sup>3+</sup> in MnO.<sup>18</sup> Indeed, in agreement with the Pourbaix diagram of manganese, it has

been shown that MnO is prone to dissolve in slightly acidic media.<sup>23</sup> To demonstrate that MnO can effectively dissolve in an Al<sup>3+</sup>-based electrolyte, we added MnO to a 2 m Al(OTf)<sub>3</sub> electrolyte (*i.e.*, the same electrolyte used in <sup>18</sup>, see Experimental Section). The resulting electrolyte was then used to cycle a fresh GLAD-ITO electrode. The results in Fig. 1C and 1D (green lines) show the successful electrodeposition/electrodissolution of MnO<sub>2</sub> under these conditions, thereby confirming the spontaneous dissolution of MnO to Mn<sup>2+</sup> in the Al<sup>3+</sup>-based electrolyte. XRF analysis of the charged electrode indicates an electrodeposited  $m_{MnO_2}$  value of 44  $\mu\text{g}\cdot\text{cm}^{-2}$ , comparable to that obtained with electrodes loaded *ex situ*. We were unable to discern aluminium in the XRF spectrum of the charged electrode, suggesting the absence of an Al<sub>x</sub>MnO<sub>2</sub> phase in contrast to what was previously reported.<sup>18</sup>

The continuous galvanostatic cycling of the GLAD-ITO electrode in the 1 M Al(OTf)<sub>3</sub> electrolyte containing 0.1 M MnCl<sub>2</sub> (see Fig. 1E and data in Table S2) demonstrates a remarkably stable and high *CE* (~97.5 % over 200 cycles), which correlates well with the stable periodic electrode absorbance variations monitored during the first 3 hours of cycling (Fig. 1F). In addition, apart from the secondary discharge plateaus that tend to progressively weaken, the galvanostatic charge/discharge curves almost overlap during cycling. These results are consistent with a complete and highly reversible electrodeposition-electrodissolution conversion process, without significant accumulation of MnO<sub>2</sub> or any other MnO<sub>x</sub> material. It is worth noting that aluminium was below the limit of quantification in all the charged and discharged electrodes investigated by XRF. This confirms that the Al<sub>x</sub>MnO<sub>2</sub> phase suggested in several works<sup>14,15,17,18</sup> is not formed and also that the electrolyte is properly removed by thoroughly rinsing the electrode with water prior to *ex situ* analysis.

We next investigated the cyclability of the MnO<sub>2</sub>-GLAD-ITO electrode in a Zn/MnO<sub>2</sub> cell configuration (two-electrode cell, see Experimental Section for details) with the electrolytes listed in Table S3 (containing Zn<sup>2+</sup> to allow for the reversible Zn<sup>2+</sup>-to-Zn conversion reaction at the anode). First, we verified that addition of 0.25 M ZnCl<sub>2</sub> to the 1 M AlCl<sub>3</sub> + 0.1 M MnCl<sub>2</sub> electrolyte does not significantly affect the reversibility and efficiency of the MnO<sub>2</sub>-to-Mn<sup>2+</sup> conversion reaction. This was confirmed from the high *CE* of the galvanostatic cycles (Fig. 2A, 2C and Table S3) and the stable absorbance change recorded during cycling (Fig. 2B). Also in this electrolyte, the Zn/MnO<sub>2</sub> cell delivers an excellent and stable discharge gravimetric capacity of ~560 mA·h·g<sub>MnO<sub>2</sub></sub><sup>-1</sup> over 100 cycles (one of the best gravimetric capacities reported for a Zn/MnO<sub>2</sub> cell). The cell also displays a remarkably high discharge voltage (~1.7 V) as well as an excellent energetic efficiency (*EE* > 80% at 10 A·g<sup>-1</sup>).

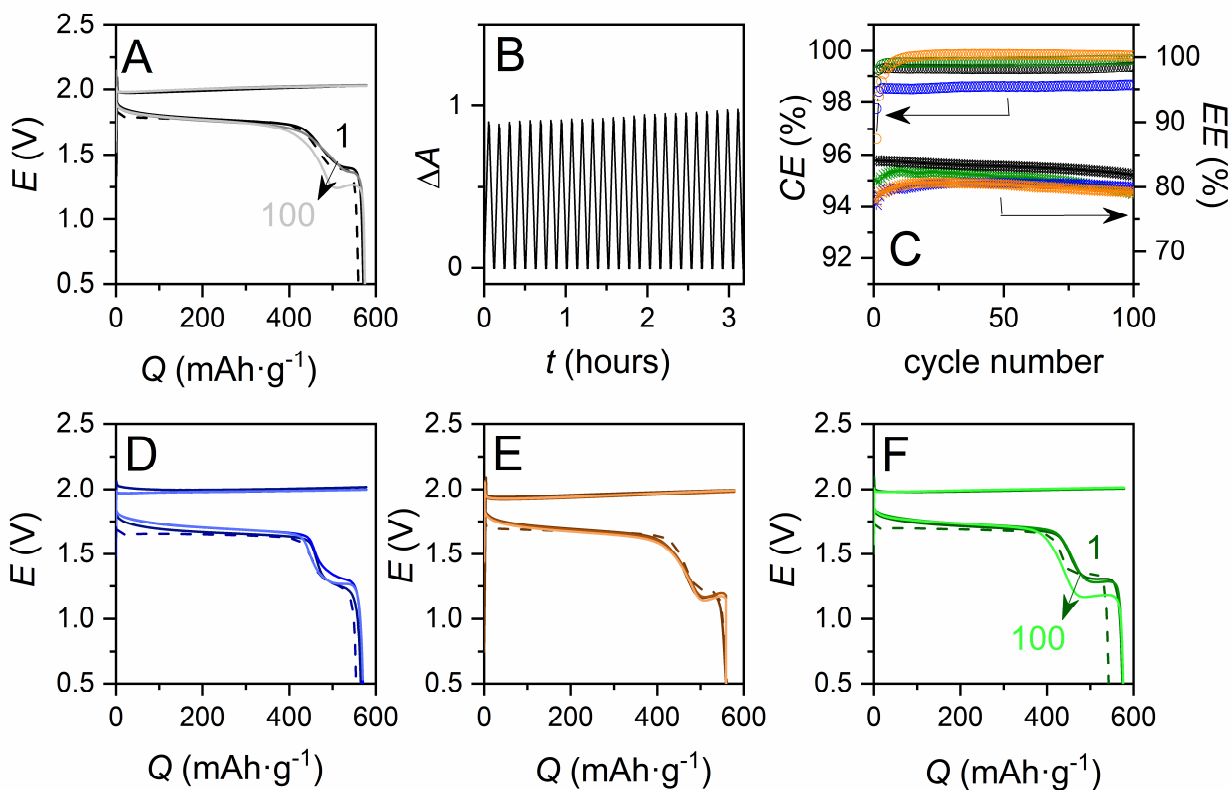
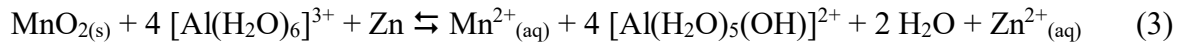


**Figure 2.** Galvanostatic cycles performed at a Zn foil/MnO<sub>2</sub>-GLAD-ITO cell assembly (loaded *ex situ* with 48 μg<sub>MnO<sub>2</sub></sub>·cm<sup>-2</sup>) in the presence of the following Al<sup>3+</sup>-based aqueous electrolytes: (A, B) 1 M AlCl<sub>3</sub> + 0.25 M ZnCl<sub>2</sub> + 0.1 M MnCl<sub>2</sub> (pH 1.90), (D) 1 M Al(OTf)<sub>3</sub> + 0.1 M ZnCl<sub>2</sub> + 0.1 M MnCl<sub>2</sub> (pH 1.77), (E) 1 M Al(OTf)<sub>3</sub> + 1 M Zn(OTf)<sub>3</sub> + 0.1 M MnSO<sub>4</sub> (pH 1.75), and (F) 1.25 M Al(OTf)<sub>3</sub> + 0.1 M ZnCl<sub>2</sub> + 0.1 M MnCl<sub>2</sub> (pH 1.5). The dashed black lines correspond to the 1<sup>st</sup> galvanostatic discharges (recorded at 0.3 mA·cm<sup>-2</sup>), while the solid lines are galvanostatic charge/discharge cycles (100 cycles at 0.5 mA·cm<sup>-2</sup> with the 1<sup>st</sup>, 50<sup>th</sup> and 100<sup>th</sup> cycles shown). (C) Cycling performances of the Zn/MnO<sub>2</sub> cell assemblies mentioned in A to F (same color code)

The data presented in Fig. 2 and Table S3 show that the chemical composition of the Al<sup>3+</sup>-based aqueous electrolytes has little effect on the shape and position of the galvanostatic charge/discharge curves. That all Zn/MnO<sub>2</sub> assemblies have such similar electrochemical features indicates they share a common charge storage mechanism that we attribute to the following dual reversible conversion process:



This mechanism is further supported by the excellent gravimetric capacity we have systematically retrieved (*i.e.* > 550 mA·h·g<sub>MnO<sub>2</sub></sub><sup>-1</sup>), which interestingly is comparable to the value recently achieved in a strongly acidic electrolyte where the reversible proton-coupled conversion of MnO<sub>2</sub> into Mn<sup>2+</sup> was fully established (see Table 1).<sup>21</sup>

We also tested a bi-cation electrolyte (1 m Al(OTf)<sub>3</sub> + 1 m Zn(OTf)<sub>2</sub> + 0.1 m MnSO<sub>4</sub>) with a composition similar to that previously used in <sup>17</sup>. Again, no significant change was observed in the charge/discharge curves (Figure 2E), which confirms that the charge storage mechanism described above remains at work. This is in sharp contrast with the previously proposed mechanism based

on the reversible co-insertion of  $H^+$  and  $Zn^{2+}$  in an  $Al_xMnO_2$  phase generated *in situ* (see further comment on pH considerations in the SI).<sup>17</sup> In such bi-cation electrolytes, the cyclability was actually improved with 100% capacity retention over 600 cycles (see Table 1), demonstrating the high reversibility of the dual conversion process.

**Table 1.** Chemical composition and pH of the aqueous electrolytes used in Zn/MnO<sub>2</sub> or Al/MnO<sub>2</sub> assemblies and the main features of the galvanostatic cycling, *i.e.* rate, half-charge ( $E_c$ ) and half-discharge ( $E_d$ ) potentials, maximal discharge capacity, and Coulombic efficiency ( $CE$ ).

electrolyte composition	pH	Anode	Rate (A·g <sup>-1</sup> )	$E_d$ (V)	$E_c$ (V)	$CE$	Maximal discharge capacity (mA·h·g <sub>MnO<sub>2</sub></sub> <sup>-1</sup> )	cathode mechanism	Ref
1 M Al(OTf) <sub>3</sub> , 0.1 M ZnCl <sub>2</sub> , 0.1 M MnCl <sub>2</sub>	1.77	Zn	10	1.65	1.99	98.8 % over 250 cycles at 10 A·g <sup>-1</sup>	560	MnO <sub>2</sub> ↔ Mn <sup>2+</sup>	This work
1 m Al(OTf) <sub>3</sub> , 1 m Zn(OTf) <sub>3</sub> , 0.1 m MnSO <sub>4</sub>	1.75	Zn	10	1.65	1.95	99.7 % over 600 cycles at 10 A·g <sup>-1</sup>	570	MnO <sub>2</sub> ↔ Mn <sup>2+</sup>	This work
1 M ZnSO <sub>4</sub> , 1 M MnSO <sub>4</sub> , 0.1 M H <sub>2</sub> SO <sub>4</sub>	1	Zn	0.58	1.95	amperometry at 2.2 V	92 % after 1800 cycles at 8.6 A·g <sup>-1</sup>	570	MnO <sub>2</sub> ↔ Mn <sup>2+</sup>	21
1 M Al(OTf) <sub>3</sub> , 1 M Zn(OTf) <sub>3</sub> , 0.1 M MnSO <sub>4</sub>	<i>ns</i>	Zn	0.1	~1.55	1.8	~100% over 1000 cycles at 1 C	264	Reversible co-insertion of Zn <sup>2+</sup> and H <sup>+</sup> in Al <sub>x</sub> MnO <sub>2</sub>	17
2 M Al(OTf) <sub>3</sub>	<i>ns</i>	Zn/Al alloy	0.1	1.6	1.8	~75% after 80 cycles at 0.1 A·g <sup>-1</sup>	460	Al <sub>x</sub> MnO <sub>2</sub> ↔ MnO with reversible uptake of Al <sup>3+</sup>	18
2 m Al(OTf) <sub>3</sub> , 0.1 m Mn(OTf) <sub>2</sub>	<i>ns</i>	T-Al	0.1	1.3	~1.6	~50% after 100 cycles at 0.2 A·g <sup>-1</sup>	310	MnO <sub>2</sub> ↔ Mn <sub>3</sub> O <sub>4</sub>	13
2 M Al(OTf) <sub>3</sub> , 0.5 M MnSO <sub>4</sub>	<i>ns</i>	T-Al	0.1	1.3→1.15	1.6	~55% after 70 cycles at 0.1 A·g <sup>-1</sup>	554	Al <sub>x</sub> Mn <sub>(1-x)</sub> O <sub>2</sub> ↔ Mn <sup>2+</sup>	15
5 M Al(OTf) <sub>3</sub>	< -0.5	Al	0.03	1.2 & 0.8	1.65	~60% after 65 cycles	467	Reversible Al <sup>3+</sup> insertion in Al <sub>x=0.1</sub> MnO <sub>2</sub>	14

*ns*: not specified

Overall, the present results shed new light on the aqueous aluminium batteries pairing a manganese oxide cathode with an aluminium or zinc anode,<sup>13-18</sup> for which the electrochemical features are gathered in Table 1. It is striking that cells based on identical anodes and electrolytes with similar pHs share similar electrochemical features (notably charge/discharge potentials), a behaviour suggesting thermodynamically equivalent electrochemical processes. On the basis of the present results, it is quite clear that  $\text{MnO}_x$  to  $\text{Mn}^{2+}$  conversion is a robust and invariable process independent of the nature of the cathode and/or electrolyte. In view of this behavior, the diversity of mechanisms proposed in the literature (summarized in Table 1) raises questions, as it is very possible that a unified mechanism drives all the Al/ $\text{MnO}_x$  or Zn/ $\text{MnO}_x$  aqueous batteries gathered in Table 1.

One may however argue that complementary material characterization techniques are required to better probe our active material and to support the proposed unified charge storage mechanism. However, the characterization techniques based on *ex situ* or *in operando* spectroscopic analysis of the charged/discharged materials, such as XRD, XPS and elemental mapping analysis, are inconveniently blind to the dissolution processes and may mislead the interpretation of the charge storage mechanism. This is especially true for the reduced state  $\text{Mn}^{2+}$ , which once solubilised in the electrolyte, is no longer detectable by such techniques. Another difficulty is linked to the amorphous state of the back electrogenerated  $\text{MnO}_x$  material, which unfortunately cannot be characterized by XRD. Despite this, several studies speculate on the *in situ* formation of a layered  $\text{Al}_x\text{MnO}_2$  phase based on the detection of Al in the XPS spectra and energy dispersive spectroscopy mappings.<sup>14,15,17,18</sup> However, this is insufficient to irrefutably demonstrate the formation of an  $\text{Al}_x\text{MnO}_2$  phase,<sup>14,15,17,18</sup> and to assert that  $\text{Al}^{3+}$  can reversibly insert into this phase.<sup>14,18</sup>

Another important aspect that is often improperly considered is that the cyclability of the Zn/MnO<sub>2</sub> batteries improves when sufficient Mn<sup>2+</sup> (0.1 to 0.5 M) is added into the Al<sup>3+</sup>-based electrolytes.<sup>13,15,17</sup> Rather than inhibiting the dissolution of Mn<sup>2+</sup>, we and other groups demonstrated that the role of pre-added Mn<sup>2+</sup> in the aqueous electrolytes is to act as a reservoir for MnO<sub>2</sub> electrodeposition during charging.<sup>12,24</sup> This is the principle of a conversion battery, where the capacity of the electrolyte has to be taken into account for the energy density calculation.

Some publications report on lower oxidation state manganese oxide cathode materials (*i.e.*, spinel Mn<sub>3</sub>O<sub>4</sub> and MnO) capable of cycling in highly concentrated Al(OTf)<sub>3</sub> aqueous electrolytes free of Mn<sup>2+</sup> ions.<sup>14,18</sup> The problem with such oxides is that they tend to spontaneously dissolve in acidic electrolytes,<sup>23,25</sup> as we have shown here with MnO. Because of the rather high concentration of Al(OTf)<sub>3</sub> used in these studies (>2 M at pH < 0, see Table S2), Mn<sup>2+</sup> is expected to be generated *in situ* from the spontaneous dissolution of the Mn<sub>3</sub>O<sub>4</sub>- or MnO-based cathode. After a certain time, a significant amount of Mn<sup>2+</sup> is thus present in these electrolytes, fulfilling the requirements for a reversible MnO<sub>2</sub>-to-Mn<sup>2+</sup> conversion.

Finally, some authors suggest the reversible insertion of multivalent cations (Al<sup>3+</sup> or Zn<sup>2+</sup>) in an *in situ* activated layered phase of Al<sub>x</sub>MnO<sub>2</sub>.<sup>14,17</sup> The present study clearly demonstrates that neither Al<sup>3+</sup> nor Zn<sup>2+</sup> can reversibly insert in the active MnO<sub>x</sub> phase, which is totally dismantled through the proton-coupled electrodisolution process.

## Conclusion

The present study unambiguously demonstrates that the reversible proton-coupled MnO<sub>2</sub>-to-Mn<sup>2+</sup> conversion is the main charge storage mechanism of MnO<sub>x</sub>-based cathodes when cycled in Al<sup>3+</sup>-based aqueous electrolytes. By avoiding excessively high concentrations of Al<sup>3+</sup> ions

associated with strongly acidic conditions, we highlighted the essential role of the  $[\text{Al}(\text{H}_2\text{O})_6]^{3+}$  complex as a proton donor, allowing exploitation of the 2 electron charge storage capacity of  $\text{MnO}_2$  with high cyclability and efficiency. The nature of the counter ions has little effect over the charge storage, making  $\text{MnO}_2$ -to- $\text{Mn}^{2+}$  conversion a robust mechanism that is was likely unknowingly involved in previous studies.

## ASSOCIATED CONTENT

(Word Style “TE\_Supporting\_Information”). **Supporting Information.** Experimental section, Supplementary Figures S1 to SX and supplementary Tables S1 to S3 are provided in the Supporting Information file.

## AUTHOR INFORMATION

### **Corresponding Authors:**

\*E-mail: [veronique.balland@u-paris.fr](mailto:veronique.balland@u-paris.fr).

\*E-mail: [limoges@u-paris.fr](mailto:limoges@u-paris.fr)

### ORCID:

Véronique Balland: 0000-0001-9534-9659

Benoît Limoges: 0000-0002-2466-1896

### **Notes**

The authors declare no competing financial interest.

## ACKNOWLEDGMENT

The authors thank Ivonne Cocca and Sophie Nowak (Université de Paris) for X-Ray fluorescence measurements. We also gratefully acknowledge financial support from the French National Agency (ANR AqReBat project).

## REFERENCES

- (1) Shin, J.; Choi, J. W. Opportunities and Reality of Aqueous Rechargeable Batteries. *Adv. Energy Mater.* **2020**, 2001386. <https://doi.org/10.1002/aenm.202001386>.
- (2) Chao, D.; Zhou, W.; Xie, F.; Ye, C.; Li, H.; Jaroniec, M.; Qiao, S. Roadmap for Advanced Aqueous Batteries : From Design of Materials to Applications. *Sci. Adv.* **2020**, *6*, eaba4098.
- (3) Park, M. J.; Asl, H. Y.; Manthiram, A. Multivalent-Ion versus Proton Insertion into Battery Electrodes. *ACS Energy Lett.* **2020**, *5*, 2367–2375. <https://doi.org/10.1021/acseenergylett.0c01021>.
- (4) Rong, Z.; Malik, R.; Canepa, P.; Sai Gautam, G.; Liu, M.; Jain, A.; Persson, K.; Ceder, G. Materials Design Rules for Multivalent Ion Mobility in Intercalation Structures. *Chem. Mater.* **2015**, *27* (17), 6016–6021. <https://doi.org/10.1021/acs.chemmater.5b02342>.
- (5) Mathew, V.; Sambandam, B.; Kim, S.; Kim, S.; Park, S.; Lee, S.; Alfaruqi, M. H.; Soundharajan, V.; Islam, S.; Putro, D. Y.; Hwang, J.; Sun, Y.; Kim, J. Manganese and Vanadium Oxide Cathodes for Aqueous Rechargeable Zinc-Ion Batteries: A Focused View on Performance, Mechanism, and Developments. *ACS Energy Lett.* **2020**, *5*, 2376–2400. <https://doi.org/10.1021/acseenergylett.0c00740>.
- (6) Manalastas, W.; Kumar, S.; Verma, V.; Zhang, L.; Yuan, D. Water in Rechargeable Multivalent-Ion Batteries : An Electrochemical Pandora’s Box. *ChemSusChem* **2019**, *12*, 379–396. <https://doi.org/10.1002/cssc.201801523>.
- (7) Liu, T.; Cheng, X.; Yu, H.; Zhu, H.; Peng, N.; Zheng, R. An Overview and Future Perspectives of Aqueous Rechargeable Polyvalent Ion Batteries. *Energy Storage Mater.* **2019**, *18* (June 2018), 68–91. <https://doi.org/10.1016/j.ensm.2018.09.027>.
- (8) Li, Z.; Ganapathy, S.; Xu, Y.; Zhou, Z.; Sarilar, M.; Wagemaker, M. Mechanistic Insight

- into the Electrochemical Performance of Zn/VO<sub>2</sub> Batteries with an Aqueous ZnSO<sub>4</sub> Electrolyte. *Adv. Energy Mater.* **2019**, *1900237*, 1–10. <https://doi.org/10.1002/aenm.201900237>.
- (9) Zhao, Q.; Liu, L.; Yin, J.; Zheng, J.; Zhang, D.; Chen, J.; Archer, L. Proton Intercalation/de-Intercalation Dynamics in Vanadium Oxides for Aqueous Aluminum Electrochemical Cells. *Angew. Chemie Int. Ed.* **2020**, *59* (n/a), 1–6. <https://doi.org/10.1002/anie.201912634>.
- (10) Park, M. J.; Manthiram, A. Unveiling the Charge Storage Mechanism in Nonaqueous and Aqueous Zn/Na<sub>3</sub>V<sub>2</sub>(PO<sub>4</sub>)<sub>2</sub>F<sub>3</sub> Batteries. *ACS Appl. Energy Mater.* **2020**, *3*, 5015–5023. <https://doi.org/10.1021/acsaem.0c00505>.
- (11) Kim, Y.-S.; Harris, K. D.; Limoges, B.; Balland, V. On the Unsuspected Role of Multivalent Metal Ions on the Charge Storage of a Metal Oxide Electrode in Mild Aqueous Electrolytes. *Chem. Sci.* **2019**, *10* (38), 8752–8763. <https://doi.org/10.1039/c9sc02397f>.
- (12) Mateos, M.; Makivic, N.; Kim, Y.-S.; Limoges, B.; Balland, V. Accessing the Two-Electron Charge Storage Capacity of MnO<sub>2</sub> in Mild Aqueous Electrolytes. *Adv. Energy Mater.* **2020**, 2000332. <https://doi.org/10.1002/aenm.202000332>.
- (13) Zhao, Q.; Zachman, M. J.; Sadat, W. I. Al; Zheng, J.; Kourkoutis, L. F.; Archer, L. Solid Electrolyte Interphases for High-Energy Aqueous Aluminum Electrochemical Cells. *Sci. Adv.* **2018**, *4* (November), eaau8131.
- (14) Wu, C.; Gu, S.; Zhang, Q.; Bai, Y.; Li, M.; Yuan, Y.; Wang, H.; Liu, X.; Yuan, Y.; Zhu, N.; Wu, F.; Li, H.; Gu, L.; Lu, J. Electrochemically Activated Spinel Manganese Oxide for Rechargeable Aqueous Aluminum Battery. *Nat. Commun.* **2019**, *10* (1), 73. <https://doi.org/10.1038/s41467-018-07980-7>.
- (15) He, S.; Wang, J.; Zhang, X.; Chen, J.; Wang, Z.; Yang, T.; Liu, Z.; Liang, Y.; Wang, B.;

- Liu, S.; Zhang, L.; Huang, J.; Huang, J.; Dell, L. A. O.; Yu, H. A High-Energy Aqueous Aluminum-Manganese Battery. *Adv. Funct. Mater.* **2019**, 1905228. <https://doi.org/10.1002/adfm.201905228>.
- (16) Joseph, J.; Nerkar, J.; Tang, C.; Du, A.; O'Mullane, A. P.; Ostrikov, K. (Ken). Reversible Intercalation of Multivalent Al<sup>3+</sup> Ions into Potassium-Rich Cryptomelane Nanowires for Aqueous Rechargeable Al-Ion Batteries. *ChemSusChem* **2019**, 12 (16), 3753–3760. <https://doi.org/10.1002/cssc.201901182>.
- (17) Li, N.; Li, G.; Li, C.; Yang, H.; Qin, G.; Sun, X.; Li, F.; Cheng, H. Bi-Cation Electrolyte for a 1.7 V Aqueous Zn Ion Battery. *ACS Appl. Mater. Interfaces* **2020**, 12, 13790–13796. <https://doi.org/10.1021/acsami.9b20531>.
- (18) Yan, C.; Lv, C.; Wang, L.; Cui, W.; Zhang, L.; Dinh, K. N.; Tan, H.; Wu, C.; Wu, T.; Ren, Y.; Chen, J.; Liu, Z.; Srinivasan, M.; Rui, X. Architecting a Stable High-Energy Aqueous Al-Ion Battery. *J. Am. Chem. Soc.* **2020**, 142, 15295615304. <https://doi.org/10.1021/jacs.0c05054>.
- (19) Mateos, M.; Harris, K. D.; Limoges, B.; Balland, V. Nanostructured Electrode Enabling Fast and Fully Reversible MnO<sub>2</sub>-to-Mn<sup>2+</sup> Conversion in Mild Buffered Aqueous Electrolytes. *ACS* **2020**, 3, 7610–7618. <https://doi.org/10.1021/acsaem.0c01039>.
- (20) Chen, W.; Li, G.; Pei, A.; Li, Y.; Liao, L.; Wang, H.; Wan, J.; Liang, Z.; Chen, G.; Zhang, H.; Wang, J.; Cui, Y. A Manganese-Hydrogen Battery with Potential for Grid-Scale Energy Storage. *Nat. Energy* **2018**, 3 (5), 428–435. <https://doi.org/10.1038/s41560-018-0147-7>.
- (21) Chao, D.; Zhou, W.; Ye, C.; Zhang, Q.; Chen, Y.; Gu, L.; Davey, K.; Qiao, S. Z. An Electrolytic Zn–MnO<sub>2</sub> Battery for High-Voltage and Scalable Energy Storage. *Angew. Chemie - Int. Ed.* **2019**, 7823–7828. <https://doi.org/10.1002/anie.201904174>.

- (22) *CRC Handbook of Chemistry and Physics*, Internet V.; Lide, D. R., Ed.; CRC Press, Boca Raton, FL, 2005.
- (23) Jones, C. F.; St, R.; Smart, C.; Turner, P. S. Dissolution Kinetics of Manganese Oxides. *J. Chem. Soc. Faraday Trans.* **1990**, *86* (6), 947–953.
- (24) Yang, J.; Cao, J.; Peng, Y.; Yang, W.; Barg, S.; Liu, Z. Unravelling the Mechanism of Rechargeable Aqueous Zn–MnO<sub>2</sub> Batteries: Implementation of Charging Process by Electrodeposition of MnO<sub>2</sub>. *ChemSusChem* **2020**, *13*, 4103–4110. <https://doi.org/10.1002/cssc.202001216>.
- (25) Artamonova, I. V.; Gorichev, I. G.; Godunov, E. B. Kinetics of Manganese Oxides Dissolution in Sulphuric Acid Solutions Containing Oxalic Acid. *Engineering* **2013**, *05* (09), 714–719. <https://doi.org/10.4236/eng.2013.59085>.

#### Overview of *ACS Energy Letters* Manuscript Format

- Page 1: Title, Authorship, Affiliations, and Corresponding Author(s)' e-mail address(es) (single page)
- Page 2: Abstract, Table of Contents Graphic (in this order, single page)
- Page 3 (onwards): Main Text including Figures, Figure Captions, Schemes, Charts, Tables and Equations where they are first mentioned
- Experimental Methods
- Associated Content, if any - Supporting Information description and Supporting Information paragraph (Note: Supporting Information should be uploaded in a file separate from the manuscript.)
- Author Information – Corresponding Author, Notes
- Acknowledgment, Funding
- References

